

Chiral meta-atoms rotated by light

Mingkai Liu, David A. Powell, and Ilya V. Shadrivov

Citation: [Applied Physics Letters](#) **101**, 031105 (2012); doi: 10.1063/1.4737441

View online: <http://dx.doi.org/10.1063/1.4737441>

View Table of Contents: <http://scitation.aip.org/content/aip/journal/apl/101/3?ver=pdfcov>

Published by the [AIP Publishing](#)

Articles you may be interested in

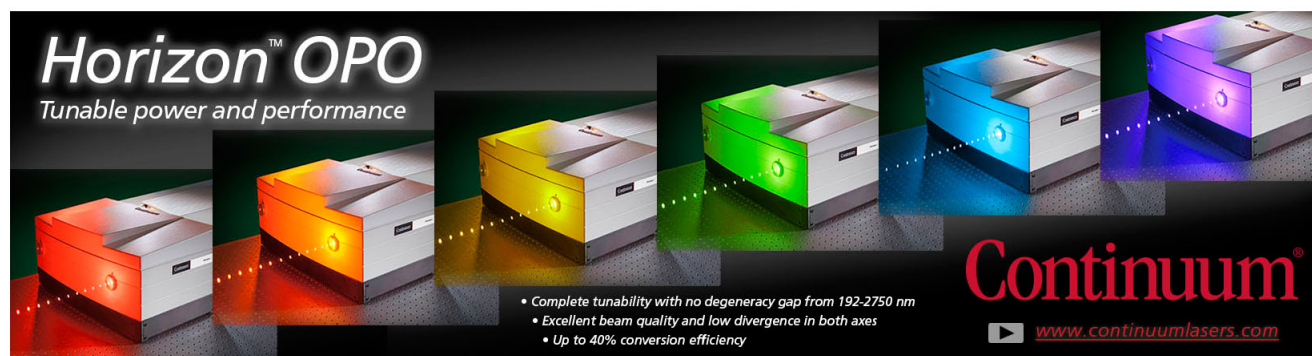
[Dual-band polarization angle independent 90° polarization rotator using twisted electric-field-coupled resonators](#)
Appl. Phys. Lett. **104**, 034102 (2014); 10.1063/1.4863227

[Complementary chiral metasurface with strong broadband optical activity and enhanced transmission](#)
Appl. Phys. Lett. **104**, 011108 (2014); 10.1063/1.4861422

[Nonlinear interaction of meta-atoms through optical coupling](#)
Appl. Phys. Lett. **104**, 014104 (2014); 10.1063/1.4861388

[A transparent 90° polarization rotator by combining chirality and electromagnetic wave tunneling](#)
Appl. Phys. Lett. **100**, 051909 (2012); 10.1063/1.3682591

[Integration of light and atom optics on an atom chip](#)
AIP Conf. Proc. **709**, 443 (2004); 10.1063/1.1764049

The advertisement features a row of five Continuum Horizon OPO laser units, each emitting a different color of light: red, orange, yellow, green, and blue. The units are arranged in a perspective view, with the blue unit on the far right. The text 'Horizon™ OPO' is prominently displayed in the top left, with the tagline 'Tunable power and performance' below it. In the bottom right, the Continuum logo is shown in red, with the website 'www.continuumlasers.com' and a play button icon. A list of features is provided in the bottom center: 'Complete tunability with no degeneracy gap from 192-2750 nm', 'Excellent beam quality and low divergence in both axes', and 'Up to 40% conversion efficiency'.

Chiral meta-atoms rotated by light

Mingkai Liu,^{a)} David A. Powell, and Ilya V. Shadrivov

Nonlinear Physics Centre, Research School of Physics and Engineering, Australian National University, Canberra, ACT 0200, Australia

(Received 17 May 2012; accepted 2 July 2012; published online 17 July 2012)

We study the opto-mechanical properties of coupled chiral meta-atoms based on a pair of twisted split-ring resonators. By using a simple analytical model in conjunction with the Maxwell stress tensor, we capture insight into the mechanism and find that this structure can be used as a general prototype of subwavelength light-driven actuators over a wide range of frequencies. This coupled structure can provide a strong and tunable torque, and can support different opto-mechanical modes, including uniform rotation, periodically variable rotation and damped oscillations. Our results suggest that chiral meta-atoms are good candidates for creating sub-wavelength motors or wrenches controlled by light. © 2012 American Institute of Physics.

[<http://dx.doi.org/10.1063/1.4737441>]

Using light to manipulate objects or even to drive a machine is fascinating. It is well known that the interaction between light and matter is usually accompanied by the transfer of momentum or angular momentum. Many tools and devices based on this principle have been developed, such as optical tweezers,^{1,2} optical wrenches,^{3,4} and optical motors.^{5,6} These light-driven tools were shown to make special contributions in the fields like micro-fluidics⁷ and biophysics.⁸ Basically, there are two ways to generate an optical torque, one is to introduce the angular momentum directly from the illuminating wave by manipulating its polarization state or phase front^{1,9,10}; another is to use chiral structures, which scatter light into different angular momentum modes with unequal intensity.^{11,12} However, due to the small dielectric constant (which also means a weak light-matter interaction) in most dielectric materials, early studies of optical torque often required birefringent or chiral structures that are of the order of (or even orders of magnitude larger than) the working wavelength to generate a sufficiently large torque.¹³ Recently, it was demonstrated that by taking advantage of the plasmonic resonance in a metallic chiral structure, a strong radiation torque can be generated with a nanoscale plasmonic motor.¹⁴

It would be inspiring progress to generate strong torque with a sub-wavelength actuator, since this is the key step towards highly integrated light-driven systems. The advent of metamaterials and plasmonic structures paves the way to achieve strong light-matter interaction within a sub-wavelength scale, and the coupled structures further offer us the chance to tune their performance through near-field interaction.^{15,16} Twisted dimers, such as twisted split-ring resonators^{17,18} and cut-wire pairs,¹⁹ are a particularly interesting class of coupled chiral meta-atoms. These chiral structures exhibit strong linear or even nonlinear optical activity near the resonances.²⁰ Although much work has been done on their electromagnetic properties, their opto-mechanical properties are still largely unexplored.

In this letter, we provide an approach to achieve a strong and tunable torque with a subwavelength chiral meta-atom. We study the radiation torque generated by a twisted splitting resonator pair (TSRRP) when illuminated by linearly polarized electromagnetic waves. With a simple analytical model based on near-field interaction, we study the mechanism and show that such structures can offer two rotational frequency bands (RFBs), in which the direction of the torque does not change as the structure rotates. The prediction from this simple model shows good overall agreement with full-wave calculations based on the Maxwell stress tensor. Moreover, we study the dynamics of this structure under the influence of friction and show that such a simple coupled structure can offer rich opto-mechanical modes, which enables the TSRRP to function as an optical motor or an optical wrench at different frequencies. Unlike the chiral structure shown in Ref. 14, the TSRRP does not rely on plasmonic resonance, and it can generate strong torques with opposite directions within a much narrower bandwidth, which further facilitate its implementation and application from microwave to optical frequency regimes.

The TSRRP studied here is illustrated in Fig. 1. The two identical SRRs (denoted as “1” and “2”) are offset by a distance s in the z direction, and the twist angle between them is fixed at θ . The incident plane wave propagates along the z axis, with a linear polarization in the x direction. Since the structure is chiral, the TSRRP may experience a radiation torque even under the illumination of linearly polarized waves, and the rotation angle is denoted as Φ . To understand the opto-mechanical properties of the structure, we first need to find its electromagnetic response, then we use its frequency-dependent charge and current distributions to calculate the radiation torque under different rotation angles, and finally we can solve the dynamic equations of the system. As our previous papers showed,^{18,19} under the single mode approximation, we can separate the current and charge of a single SRR into a frequency-dependent mode amplitude $Q_m(\omega)$ ($m = 1, 2$) and spatial distributions $\mathbf{j}(\mathbf{r})$ and $q(\mathbf{r})$. To describe the coupling of the system, the following coupled equations are employed,

^{a)} Author to whom correspondence should be addressed. Electronic mail: lmk124@physics.anu.edu.au.

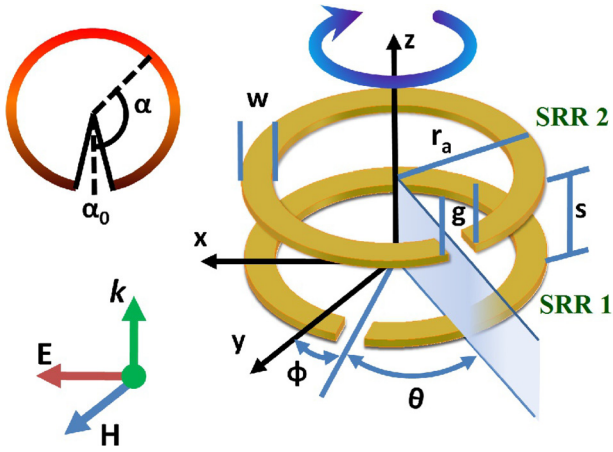


FIG. 1. Schematic layout of the TSRRP. The centre-centre distance between the two coaxial SRRs is s . The resonators are fixed with respect to each other, and the twist angle is θ . A linearly polarized plane wave propagates along the z direction. The TSRRP rotates about the z axis, with the rotation angle denoted as Φ . The red curve denotes the line-current model of a SRR, where α is the azimuthal angle and α_0 is the angle of the gap width.

$$\begin{aligned} Q_1(1/C_{11} - \omega^2 L_{11}) + Q_2(1/C_{12} - \omega^2 L_{12}) &= -\mathbf{E} \cdot \mathbf{l}_{eff} \\ Q_1(1/C_{21} - \omega^2 L_{21}) + Q_2(1/C_{22} - \omega^2 L_{22}) &= -\mathbf{E} \cdot \mathbf{l}_{eff} \cdot e^{i\varphi}, \end{aligned} \quad (1)$$

where \mathbf{E} is the incident electric field, $l_{eff} = |\int_{V_m} q(\mathbf{r}) \mathbf{r} d^3 \mathbf{r}|$ is the effective dipole length and $\varphi = k_0 s$ is the retardation along the propagation direction. C_{mn} and L_{mn} ($m, n \in [1, 2]$) are related to the effective capacitance and inductance, and can be defined by the near-field interaction terms.¹⁹ Note that for two identical SRRs, $C_{11} = C_{22}$, $C_{12} = C_{21}$, and $L_{11} = L_{22}$, $L_{12} = L_{21}$. The mode amplitudes can then be written in a compact form,

$$Q_1 = (V_2 F_m - V_1 F_s) / (F_s^2 - F_m^2) \quad (2)$$

$$Q_2 = (V_1 F_m - V_2 F_s) / (F_s^2 - F_m^2). \quad (3)$$

$V_1(\Phi) = \mathbf{E} \cdot \mathbf{l}_{eff} = |E| l_{eff} \sin \Phi$, $V_2(\Phi) = \mathbf{E} \cdot \mathbf{l}_{eff} \cdot e^{i\varphi} = |E| l_{eff} \sin(\Phi + \theta) \cdot e^{i\varphi}$ correspond to the effective voltage applied to the SRRs by the incident field, and $F_s = 1/C_{11} - \omega^2 L_{11}$, $F_m = 1/C_{12} - \omega^2 L_{12}$ are the self/mutual interaction terms. To start with, we treat each SRR as an infinitely thin current line, with a sinusoidal current distribution,

$$\mathbf{j}(\alpha) = \begin{cases} 0, & \alpha \in \left[-\frac{\alpha_0}{2}, \frac{\alpha_0}{2}\right] \\ \hat{\mathbf{e}}_\alpha \cdot \sin\left[\frac{(\alpha - \alpha_0/2)\pi}{2\pi - \alpha_0}\right], & \alpha \notin \left[-\frac{\alpha_0}{2}, \frac{\alpha_0}{2}\right] \end{cases}. \quad (4)$$

α is the azimuthal angle and α_0 is the angle of the gap, as shown in Fig. 1; the charge spatial distribution can be obtained from

$$q(\alpha) = -\nabla \cdot \mathbf{j}(\alpha) = -\frac{1}{r_a} \frac{\partial}{\partial \alpha} j(\alpha)$$

with r_a being the radius of the SRR. The effective capacitance and inductance, as well as the mode amplitudes can be worked out following the above procedure. Once we get the frequency-dependent current and charge distributions

$\mathbf{J}(\mathbf{r}, \omega) = -j\omega Q(\omega) \mathbf{j}(\mathbf{r})$ and $\rho(\mathbf{r}, \omega) = Q(\omega) q(\mathbf{r})$, we can calculate the torque experienced by each of the SRRs, and their sum is the net external torque. The torque induced by the external field is

$$\mathbf{M}_{ext} = \int_V \mathbf{r} \times [\rho(\mathbf{r}) \mathbf{E} + \mathbf{J}(\mathbf{r}) \times \mathbf{B}] d^3 \mathbf{r}. \quad (5)$$

We assume that the structure is only allowed to rotate about the z axis. Due to the structural symmetry, the magnetic part does not contribute to the torque about the z axis. The time averaged torque exerted on SRR 1 and 2 can then be written in a very concise form,

$$\mathbf{M}_{ext,1} = -\frac{1}{2} Re[Q_1^*(\omega, \Phi)] l_{eff} |E| \sin \Phi \cdot \hat{\mathbf{z}} \quad (6)$$

$$\mathbf{M}_{ext,2} = -\frac{1}{2} Re[Q_2^*(\omega, \Phi) e^{i\varphi}] l_{eff} |E| \sin(\Phi + \theta) \cdot \hat{\mathbf{z}}. \quad (7)$$

By substituting Eqs. (2) and (3) into Eqs. (6) and (7), we finally arrive at the total external torque

$$\mathbf{M}_{ext} = \mathbf{M}_{ext,1} + \mathbf{M}_{ext,2} = \mathbf{M}_o + \mathbf{M}_r, \quad (8)$$

where

$$\mathbf{M}_o = \frac{l_{eff}^2 |E|^2}{2} Re(A^* \cos \theta - B^* \cos \varphi) \sin(2\Phi + \theta) \cdot \hat{\mathbf{z}} \quad (9)$$

$$\mathbf{M}_r = \frac{l_{eff}^2 |E|^2}{2} Im(B^*) \sin \theta \sin \varphi \cdot \hat{\mathbf{z}} \quad (10)$$

with $A = F_s / (F_s^2 - F_m^2)$ and $B = F_m / (F_s^2 - F_m^2)$. Note that A and B are independent of the rotation angle Φ . Thus, the above two equations clearly demonstrate that the total torque is actually composed of two parts. One is a rotation angle-dependent torque $\mathbf{M}_o(\Phi)$, whose sign is periodically changing as the structure rotates, and thus it leads to the oscillatory dynamics. The component \mathbf{M}_r does not depend on Φ and it contributes to a continuous rotation. We further note that \mathbf{M}_r vanishes when any of the following three go to zero: the mutual interaction F_m , the retardation φ or the twist angle θ , which verifies its relation with the structural chirality. It can be expected that there will be a RFB when $M_{diff} = |\mathbf{M}_r| - \max(|\mathbf{M}_o|) > 0$, in which the TSRRP will be driven to rotate continuously in one direction.

To verify our prediction, we compare the results from full wave simulation (CST Microwave Studio). In the analytical model, we choose $r_a = 1.16$ mm and $\alpha_0 = 11^\circ$. In the full wave simulation, we calculate the structures that work in microwave and optical frequencies, respectively. For the microwave sample, the metal is chosen as copper ($\sigma = 5.8 \times 10^7$ S/m) and the background is vacuum; while for the optical sample, the metal is gold described by the Drude model ($\epsilon_\infty = 1$, $\omega_p = 1.37 \times 10^{16}$ rad/s, $\Gamma = 1.2 \times 10^{14}$ Hz) and the background is set as SiO_2 ($\epsilon_r = 2.13$). The external torque is calculated via the Maxwell stress tensor.²¹ Since any linear-polarization can be decomposed into two orthogonal components, we calculate the torque under $\Phi = 0^\circ$ and 90° , to confirm the position of the RFBs.

Remarkably, for the microwave sample, both the trends of the normalized mode amplitudes and the torques show good overall agreement with our simple model, as shown in Figs. 2(a)–2(d). The differences might arise from the actual geometries of the structures and some perturbation of the charge and current distributions due to strong near-field interaction. For the optical sample [Figs. 2(e) and 2(f)], the simple model (not shown) gives only qualitative agreement, due to the neglect of the metal dispersion. However, the numerical results confirm that the physics is the same for the microwave and optical regimes.

The values in Figs. 2(b) and 2(d) are normalized to an input power density of 1 mW/mm^2 ; in Fig. 2(f), the values are normalized to a power density of $1 \text{ mW}/\mu\text{m}^2$. The two resonances around 19.6 GHz (205 THz) and 20.8 GHz (250 THz) correspond to the symmetric mode and antisymmetric mode, respectively. We note from Figs. 2(b), 2(d), and 2(f) that there are two RFBs around the resonances, which are denoted by the blue and red shadings: in the blue area (the lower frequency bands), M_{ext} is always negative; while in the red area (the higher frequency bands), M_{ext} is always positive. Such agreement demonstrates that the simple analytical model of the TSRRP can be used for calculating and designing subwavelength light-driven actuators over a wide range of frequencies. Moreover, it is quite inspiring that the

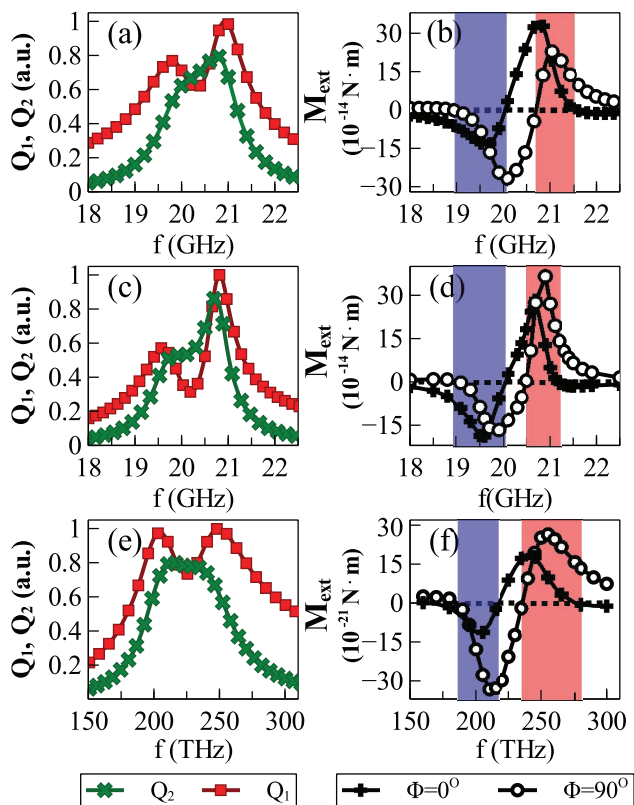


FIG. 2. Normalized mode amplitudes Q_1 , Q_2 and the radiation torque M_{ext} of the TSRRP with $\theta = 90^\circ$, where (a) and (b) are calculated from the analytical model, (c) and (d) are the full wave calculations of the microwave sample, and (e) and (f) are the full wave calculations of the optical sample. For the analytical model, $r_a = 1.16 \text{ mm}$, $\alpha_0 = 11^\circ$; for the microwave sample, $r_a = 1.2 \text{ mm}$, metal thickness $t = 0.03 \text{ mm}$, $w = 0.24 \text{ mm}$, $g = 0.2 \text{ mm}$, and $s = 2 \text{ mm}$; for the optical sample, $r_a = 80 \text{ nm}$, $t = 30 \text{ nm}$, $w = 30 \text{ nm}$, $g = 30 \text{ nm}$, and $s = 80 \text{ nm}$. The blue and red shadings in the torque diagrams denote the RFBs.

torque calculated from the unoptimized subwavelength ($\approx \lambda^3/500$) optical sample is of the order of $2 \times 10^{-20} \text{ N} \cdot \text{m}$, which is comparable to that shown in previous works which use much larger dielectric chiral structures ($> 25\lambda^3$) and higher power trapping beams.¹³

In contrast to the optical motor based on a single resonator, the TSRRP enables us to tune its resonant properties and opto-mechanical behaviour, by changing the geometry of the resonators. To capture insight into the evolution of the RFBs as the twist angle θ and the separation s change, we plot $M_{\text{diff}} > 0$ as a function of frequency and θ in Figs. 3(a) and 3(b) by fixing $s = 1 \text{ mm}$ and $s = 2 \text{ mm}$; in Figs. 3(c) and 3(d), s varies from 0.5 mm to 3.5 mm, while θ is fixed at 45° and 90° , respectively. The regimes with $M_{\text{diff}} > 0$ correspond to the RFBs. Through the tuning, we can change the bandwidths, spectral distance and the strength of the two bands.

When carefully examining the evolution of the RFBs, one feature attracts our attention: although the RFBs centre around the two branches of resonances, the variation of their bandwidths and the rotating power does not coincide with the change of the resonances. For the TSRRP we study, the bandwidth of the symmetric mode exhibits a monotonic decrease as the twist angle or separation increases, while a reversed trend can be observed for the antisymmetric mode.¹⁸ However, the bandwidths of RFBs show a more complicated non-monotonic behaviour since it is affected by several factors. For a given twist angle or separation, there is an optimum configuration in which we can get the strongest rotational power, as shown by the white arrows in Fig. 3. Qualitatively, we can understand this behaviour from Eq. (10): the strength of M_r is simultaneously affected by the mutual interaction F_m , the retardation φ and the twist angle θ . To take the antisymmetric mode as an example, decreasing the separation or twist angle usually gives a stronger resonance, however, this comes at the expense of smaller

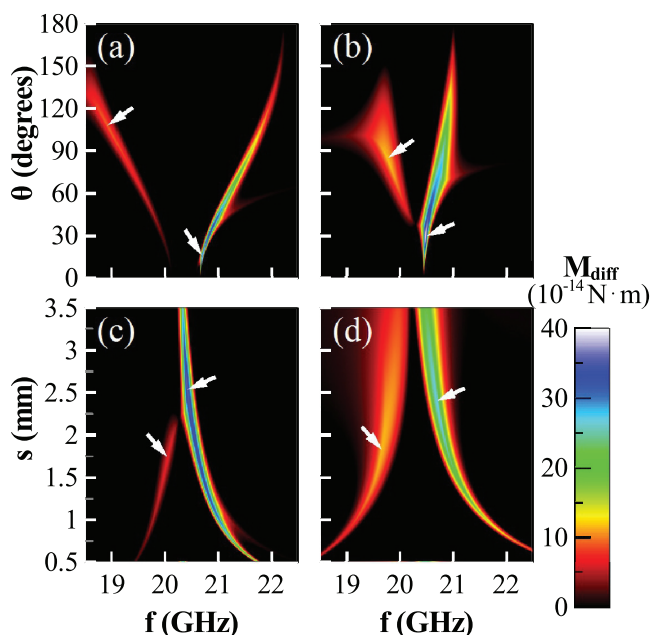


FIG. 3. The frequency bands of continuous rotation as a function of θ and s , determined from the condition $M_{\text{diff}} > 0$. (a) $s = 1 \text{ mm}$, (b) $s = 2 \text{ mm}$, (c) $\theta = 45^\circ$, and (d) $\theta = 90^\circ$. The white arrows indicate the optimum points.

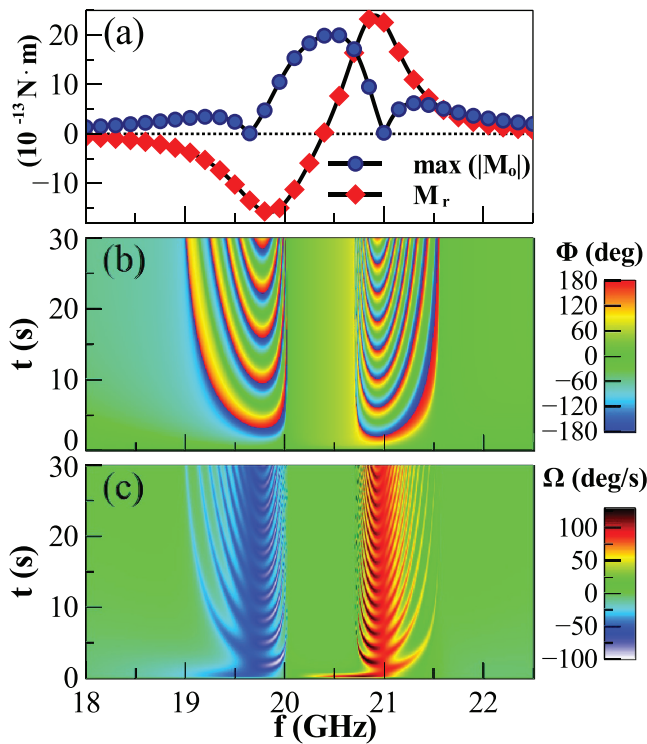


FIG. 4. Dynamics of the TSRRP with air friction, under an illumination power density of 10 mW/mm^2 . (a) \mathbf{M}_r and $\max(|\mathbf{M}_o|)$, (b) rotation angle Φ , and (c) angular speed Ω as a function of pump frequency and time.

values of $\sin \theta$ and $\sin \Phi$, thus the optimum configuration should be a balance of the resonance strength, the degree of asymmetry and the retardation.

Using the analytical expression for the torque, we study the dynamics of the structure also taking into account friction in the system, which can be caused by the medium in which the meta-atom is placed. Here, we suppose the TSRRP is fixed in a solid disk with radius $R = 2 \text{ mm}$, and the whole structure is suspended in air. The angular speed $\Omega = \dot{\Phi}(t)$ of the TSRRP can be found from the dynamic equation using, e.g., numerical Runge-Kutta method

$$I\ddot{\Phi} + \gamma\dot{\Phi} = M_{ext}(\Phi), \quad (11)$$

where I is the moment of inertia of the structure, $\gamma = \pi R^2 \eta (4R/3 + 2s)$ is the damping coefficient, which for the case of air viscosity $\eta = 17.8 \mu\text{Pa}\cdot\text{s}$. The introduction of additional friction may change the rotational velocity, but will not change the overall dynamic characteristics. Fig. 4 depicts the torque components \mathbf{M}_r and $\max(|\mathbf{M}_o|)$ as well as the rotation dynamics of the TSRRP with parameters corresponding to Figs. 2(a) and 2(b), and the incident power flow is 10 mW/mm^2 . As expected, two RFBs with opposite rotation directions appear near the symmetric and antisymmetric resonances, with their regimes determined by $|\mathbf{M}_r| > \max(|\mathbf{M}_o|)$, as predicted in Fig. 2(b).

The TSRRP will experience a continuous rotation when driven by a frequency within the RFBs, and thus it can act as a subwavelength motor; while outside the RFBs, the rotation angle becomes stable after a relaxation process, and the

structure behaves as an anisotropic scatter and can function as an optical wrench. The scattered wave amplitude also changes periodically as the structure rotates, and thus it provides the possibility to detect its motion and the torque. In contrast to chiral structures with high degree of rotational symmetry or simple anisotropic structures, the TSRRP can offer a variety of opto-mechanical modes: (1) rotation with constant speed, which can be obtained around the point $\max(|\mathbf{M}_o|) \rightarrow 0$; (2) rotation with time-varying speed (which means one can accelerate and decelerate the structure repeatedly), with its variation periods determined by the frequency; (3) damped oscillations, in which one can control the equilibrium position by changing the input polarization angle or the frequency. Such multifunctional subwavelength light-driven actuator can potentially find a variety of applications in nano-fluidics and nano-robotics.

To conclude, we propose to use a pair of twisted SRRs as an efficient subwavelength optical actuator. By using a simple analytical model and full wave numerical simulations, we studied its mechanism and showed that this structure can be used as a general design prototype in a wide frequency range from microwaves to optics. Such a coupled structure provides strong rotational power and multiple opto-mechanical modes, which can be more easily tuned by incident frequency than other structures like metallic gamadions, and thus benefiting its application in a variety of fields.

The authors thank Miss Y. Sun for the fruitful discussion on the Maxwell stress tensor. This work is supported by the Australian Research Council.

- ¹D. G. Grier, *Nature* **424**, 810 (2003).
- ²J. R. Moffitt, Y. R. Chemla, S. B. Smith, and C. Bustamante, *Annu. Rev. Biochem.* **77**, 205 (2008).
- ³A. La Porta and M. D. Wang, *Phys. Rev. Lett.* **92**, 190801 (2004).
- ⁴F. Pedaci, Z. Huang, M. van Oene, S. Barland, and N. Dekker, *Nature Phys.* **7**, 259 (2010).
- ⁵P. Galajda and P. Ormos, *Appl. Phys. Lett.* **78**, 249 (2001).
- ⁶L. Kelemen, S. Valkai, and P. Ormos, *Appl. Opt.* **45**, 2777 (2006).
- ⁷M. Barbic, J. J. Mock, A. P. Gray, and S. Schultz, *Appl. Phys. Lett.* **79**, 1399 (2001).
- ⁸F. M. Fazal and S. M. Block, *Nature Photon.* **5**, 318 (2011).
- ⁹P. Allen, *Amer. J. Phys.* **74**, 1185 (1966).
- ¹⁰S. Franke-Arnold, L. Allen, and M. Padgett, *Laser & Photon. Rev.* **2**, 299 (2008).
- ¹¹P. Galajda and P. Ormos, *Appl. Phys. Lett.* **80**, 4653 (2002).
- ¹²T. Nieminen, S. Parkin, N. Heckenberg, and H. Rubinsztein-Dunlop, *Optical Trapping and Optical Micromanipulation* (SPIE, 2011), pp. 254–263.
- ¹³W. L. Collett, C. A. Ventrice, and S. M. Mahajan, *Appl. Phys. Lett.* **82**, 2730 (2003).
- ¹⁴M. Liu, T. Zentgraf, Y. Liu, G. Bartal, and X. Zhang, *Nature Nanotechnol.* **5**, 570 (2010).
- ¹⁵B. Luk'yanchuk, N. I. Zheludev, S. A. Maier, N. J. Halas, P. Nordlander, H. Giessen, and C. T. Chong, *Nature Mater.* **9**, 707 (2010).
- ¹⁶N. J. Halas, S. Lal, W. S. Chang, S. Link, and P. Nordlander, *Chem. Rev.* **111**, 3913 (2011).
- ¹⁷N. Liu, H. Liu, S. Zhu, and H. Giessen, *Nature Photon.* **3**, 157 (2009).
- ¹⁸D. A. Powell, K. Hannam, I. V. Shadrivov, and Y. S. Kivshar, *Phys. Rev. B* **83**, 235420 (2011).
- ¹⁹M. Liu, D. A. Powell, I. V. Shadrivov, and Y. S. Kivshar, *Appl. Phys. Lett.* **100**, 111114 (2012).
- ²⁰I. V. Shadrivov, V. A. Fedotov, D. A. Powell, Y. S. Kivshar, and N. I. Zheludev, *New J. Phys.* **13**, 033025 (2011).
- ²¹J. Jackson and R. Fox, *Classical Electrodynamics* (Wiley, 1999).